



HAL
open science

Reaction kinetics of 1,4-cyclohexadienes with OH radicals: an experimental and theoretical study

Binod Raj Giri, Tam V.-T. Mai, Mohamed Assali, Thi T.-D. Nguyen, Hieu Nguyen, Milán Szóri, Lam Huynh, Christa Fittschen, Aamir Farooq

► **To cite this version:**

Binod Raj Giri, Tam V.-T. Mai, Mohamed Assali, Thi T.-D. Nguyen, Hieu Nguyen, et al.. Reaction kinetics of 1,4-cyclohexadienes with OH radicals: an experimental and theoretical study. *Physical Chemistry Chemical Physics*, 2022, 24 (13), pp.7836-7847. 10.1039/D1CP04964J . hal-03853289

HAL Id: hal-03853289

<https://hal.science/hal-03853289v1>

Submitted on 15 Nov 2022

HAL is a multi-disciplinary open access archive for the deposit and dissemination of scientific research documents, whether they are published or not. The documents may come from teaching and research institutions in France or abroad, or from public or private research centers.

L'archive ouverte pluridisciplinaire **HAL**, est destinée au dépôt et à la diffusion de documents scientifiques de niveau recherche, publiés ou non, émanant des établissements d'enseignement et de recherche français ou étrangers, des laboratoires publics ou privés.

Reaction Kinetics of 1,4-Cyclohexadienes with OH Radicals: An Experimental and Theoretical Study

Binod Raj Giri,¹ Tam V.-T. Mai^{2,3,4}, Mohamed Assali⁵, Thi T.-D. Nguyen^{4,6}, Hieu T. Nguyen², Milán Szóri⁷, Lam K. Huynh^{*4,6}, Christa Fittschen^{*5} and Aamir Farooq¹

¹King Abdullah University of Science and Technology (KAUST), Clean Combustion Research Center, Physical Sciences and Engineering Division, Thuwal 23955-6900, Saudi Arabia

² Molecular Science and Nano-Materials Lab, Institute for Computational Science and Technology, SBI Building, Quang Trung Software City, Tan Chanh Hiep Ward, District 12, Ho Chi Minh City, Vietnam.

³ University of Science, Vietnam National University – HCMC, 227 Nguyen Van Cu, Ward 4, District 5, Ho Chi Minh City, Vietnam.

⁴ Vietnam National University – HCMC, Quarter 6, Linh Trung Ward, Thu Duc District, Ho Chi Minh City, Vietnam.

⁵ Université Lille, CNRS, UMR 8522 - PC2A - Physicochimie des Processus de Combustion et de l'Atmosphère, F-59000 Lille, France

⁶ International University, Quarter 6, Linh Trung Ward, Thu Duc District, Ho Chi Minh City, Vietnam.

⁷ Institute of Chemistry, Faculty of Materials Science and Engineering, University of Miskolc, Hungary

*Corresponding authors' email: hklam@hcmiu.edu.vn

christa.fittschen@univ-lille.fr

Abstract

This work presents OH-initiated oxidation kinetics of 1,4-cyclohexadiene (1,4-CHD). Temperature dependence of the reaction was investigated by utilizing laser flash photolysis flow reactor and laser-induced fluorescence (LPFR/LIF) technique over the temperature range of 295 – 438 K and pressure of ~ 50 Torr. The kinetics of the reaction was followed by measuring the LIF signal of OH radicals near 308 nm. The reaction of OH radicals with 1,4-CHD exhibited a clear negative temperature dependence. To discern the role of various channels, ab initio and RRKM-based ME calculations (RRKM-ME) were performed over temperatures of 200 – 2000 K and pressures of 0.76 – 7600 Torr. The computed energy profile revealed that the reaction proceeds via the formation of a pre-reaction van der Waal complex at the entrance channel. The complex was found to be more stable than that usually seen in other alkenes + OH reactions. Both the addition channel and the abstraction reaction of allylic hydrogen were found to have negative energy barriers. Interestingly, the abstraction reaction exhibited a negative temperature dependence at low temperatures and contributed significantly (~37%) to the total rate coefficients even under atmospheric conditions. At $T \geq 900$ K, the reaction was found to proceed exclusively (> 95%) via the abstraction channel. Due to the competing channels, the reaction of OH radicals with 1,4-CHD displays complicated kinetic behaviours, reflecting the salient features of the energy profile. The role of competing channels was fully characterized by our kinetic model. The calculated rate coefficients showed an excellent agreement with the available experimental data.

1. Introduction

The formation of the first aromatic ring is key to understand the growth rates of polycyclic aromatic hydrocarbons (PAHs) and soot formation processes.^{1, 2} Several mechanisms, such as hydrogen abstraction acetylene addition (HACA)³⁻⁵, hydrogen abstraction vinylacetylene addition (HAVA)⁶, and phenyl addition dehydrocyclization (PAC)⁷ have been proposed in literature for the growth of PAHs. In these mechanisms, phenyl radicals derived from benzene are ubiquitous. Therefore, exploration of the chemical pathways forming “benzene” is critical for the mechanistic understanding of soot formation processes.

It is a well-known fact that small resonantly stabilized radicals (RSRs) such as propargyl (C_3H_3) and allyl (C_3H_5) are largely responsible for benzene formation. These RSRs are thermodynamically more stable than their saturated counterparts.⁸ Consequently, they are formed faster and undergo slower destruction under combustion-relevant conditions. Self-recombination and cross-reactions of these RSRs are believed to be the main source of benzene in hydrocarbon flames. An alternate chemical pathway involving a stepwise dehydrogenation of C6-cyclic hydrocarbons leading to benzene formation has also been proposed in literature. This pathway contributes significantly to the formation of benzene during pyrolysis and/or oxidation of cyclic hydrocarbons and/or alkenes under fuel-rich conditions.^{2, 9-13} For this pathway, cyclohexadienyl radical ($c-C_6H_7$) is an important intermediate species which liberates an H atom to yield benzene ($c-C_6H_6$). Li et al.¹¹ reported that the chemical pathway via cyclohexadienyl radical contributes almost exclusively to benzene formation in cyclohexane flames under stoichiometric conditions. Under fuel-rich conditions, they reported that direct H_2 elimination from cyclohexadienes forming benzene (i.e., $c-C_6H_8 \rightarrow c-C_6H_6 + H_2$) is also important. Wang et al.¹⁰ also highlighted the

importance of dehydrogenation reactions of cyclohexadienes accounting for the majority of benzene formation during the pyrolysis of cyclohexene and 1,5-hexadiene. Similarly, Nagaraja et al.¹³ reported that benzene formation predominantly happens via fulvene in isobutene pyrolysis where cyclopentadienyl radical plays a critical role; likewise, 4% of the benzene formation occurs via cyclohexadiene channel in 2-butene pyrolysis. The authors reported that ~99% of cyclohexadienyl radicals are formed via fulvene pathway in isobutene and 2-butene pyrolysis. Therefore, cyclohexadienyl radicals play an important role in soot formation processes during the pyrolysis and oxidation of olefinic fuels. It is well-known that olefins are vital intermediates in the oxidation of alkanes and practical fuels.

Olefins are extremely important in atmospheric chemistry. Many olefinic compounds, including cyclic and acyclic dienes, are emitted in large quantities into the earth's atmosphere from both biogenic and anthropogenic sources, e.g., automobile emissions, evaporation of transportation fuels, forest fires, biogenic isoprenes, and terpenes.¹⁴ It is well-known that OH-initiated oxidation of olefins is one of the main pathways dictating the fate of these compounds in the atmosphere. The reactivity of hydrocarbons with OH radicals in the atmosphere also affects ozone formation. The atmospheric chemistry of diolefins is fascinating as they offer more reaction pathways with OH radicals than mono-olefins. Consequently, one can speculate that OH-initiated oxidation of diolefins such as cyclic olefins followed by the reactions with other atmospheric oxidants (O_2 , O_3 , NO_x) can lead to the formation of a wide array of highly-oxidized organic species. These reactions can contribute to secondary organic aerosols (SOA) in the atmosphere. The mechanism for SOA formation is quite complex, with multiple channels and steps. Therefore, reactions of cyclic dienes

with hydroxyl radicals constitute an important reaction class for both atmospheric and combustion systems.

Reactions of olefins with OH are probably one of the most critical reaction routes for enol inception. Taatjes and co-workers^{15, 16} have highlighted the importance of enol formation during hydrocarbon oxidation in atmospheric and combustion environments. They reported unexpectedly high concentrations of C2 – C4 enols as intermediates during hydrocarbon oxidation which could not be accounted for by the existing combustion chemistry models. Similarly, the current understanding of atmospheric chemistry models cannot account for the exceptionally high concentrations of organic acids observed in the urban troposphere. Because of the importance of unexpected chemical compounds such as enols, our work explored the reactions of 1,4-cyclohexadiene (1,4-CHD) with OH radicals forming an adduct radical which may undergo beta-scission (H-elimination) to produce cyclic enols. For diolefins + OH reactions, the possibility for the enol formation can be higher as opposed to the mono-olefin + OH reactions since the incipient adduct radicals are resonantly stabilized, and they can survive longer times even at higher temperatures. Such a scenario provides a more likelihood of opening new reaction pathways, e.g., non-abstraction bimolecular reactions leading to enols formation. However, the degree of importance of enol formation is likely to be olefinic fuel-specific.

Recently, we reported high-temperature rate coefficients for the reactions of 1,3- cyclohexadiene (1,3-CHD) and 1,4- cyclohexadiene (1,4-CHD) with OH radicals.¹⁷ These reactions were investigated in a shock tube using UV laser absorption over the temperature range of 900 – 1100 K and pressures of ~ 1-3 bar. We found that both isomers exhibit similar reactivity with OH

radicals at high temperatures, and the measured rate coefficients showed a weak temperature dependence and no discernible pressure dependence. On the contrary, at 298 K, the reaction of OH radicals with 1,3-CHD was found to exhibit a factor of 1.7 higher reactivity than that of 1,4-CHD.^{18,19} Interestingly, both isomers showed a large drop in the rate coefficients from room temperature to high temperatures, e.g., for OH + 1,4-CHD reaction, $k(\sim 1030\text{ K})^{17} = 3.8 \times 10^{-11}\text{ cm}^3\text{ molecule}^{-1}\text{ s}^{-1}$ vs. $k(298\text{ K})^{18} = (9.86 \pm 0.31) \times 10^{-11}\text{ cm}^3\text{ molecule}^{-1}\text{ s}^{-1}$ and $k(298\text{ K})^{19} = (9.48 \pm 0.39) \times 10^{-11}\text{ cm}^3\text{ molecule}^{-1}\text{ s}^{-1}$.

For alkenes + OH reactions, it is a well-known fact that hydrogen abstraction reactions prevail at high temperatures, whereas OH addition to the double bond of alkenes contributes almost exclusively at low temperatures with some exceptions. The temperature range at which the addition channel shows the dominance can depend on the olefin's carbon-chain length. When the carbon chain of olefin increases, the supremacy of the addition channel further shifts to a lower temperature as more abstractable hydrogen atoms are available in the system, e.g., $T < 900\text{ K}$ for $\text{C}_2\text{H}_4 + \text{OH}^{20}$ and $T < 700\text{ K}$ for $\text{C}_3\text{H}_6 + \text{OH}^{21}$ chemical systems at 760 Torr. As for 1,3-CHD and 1,4-CHD reactions with OH radicals, hydrogen abstraction reaction from the allylic site yields resonantly stabilized cyclohexa-2,5-dien-1-yl radical (*c*-C₆H₇). In our earlier work,¹⁷ we found that hydrogen abstraction reaction is highly exothermic ($\Delta_r H^\circ(298.15\text{ K}) \sim -174.0\text{ kJ/mol}$) which is comparable to that of OH addition to 1,3-CHD forming 6-hydroxycyclohex-2-en-1-yl ($\Delta_r H^\circ(298.15\text{ K}) = -179.2\text{ kJ/mol}$). We found the reaction exothermicity of OH addition to 1,4-CHD, forming 6-hydroxycyclohex-3-en-1-yl ($\Delta_r H^\circ(298.15\text{ K}) = -111.9\text{ kJ/mol}$), to be significantly lower. Interestingly, we found that the transition states pertinent to allylic hydrogen abstraction of 1,3-CHD and 1,4-CHD are submerged below the reactants' energy, having a

negative barrier of $\Delta E_0 = -6.9$ kJ/mol and -13.7 kJ/mol, respectively. The occurrence of a negative energy barrier for the hydrogen abstraction reaction is not so common. As a result of the submerged barrier, the hydrogen abstraction from the allylic C-H site can exhibit an unusual negative T -dependence. From these observations, one can speculate that a large percentage of the reaction flux can go through hydrogen abstraction channel even at low temperatures. Although this hypothesis appears to contradict the conventional knowledge of OH + alkenes reactions, it looks plausible. Such chemical systems are quite complex in nature due to several competing channels. However, the complex kinetics of such systems can be characterized with the help of a combined experimental and theoretical study.

The current work focuses on 1,4-CHD + OH reaction with the following objectives:

- (i) Measuring the temperature dependence of the rate coefficients, $k(T)$, in a flow reactor by using laser flash photolysis and laser-induced fluorescence (LPFR/LIF) technique. To our knowledge, this is the first experimental determination of $k(T)$ of 1,4-CHD + OH reaction at low temperatures.
- (ii) Characterizing the salient features of OH radical reaction with 1,4-CHD by exploring the potential energy surface (PES) using ab initio methods.
- (iii) Rationalizing the importance of various channels in the PES of OH + 1,4-CHD using RRKM-ME calculations for total and channel-specific rate coefficients, $k(T, p)$. Again, this is the first computational study providing a detailed kinetic picture of OH + 1,4-CHD.

2. Experimental Method

The experiments were performed in a flow reactor utilizing laser-flash photolysis coupled to a high repetition rate laser-induced fluorescence (LPFR/LIF) technique over the temperature range of 295 – 439 K and pressure near 50 Torr. Details of the experimental setup and data treatment can be found elsewhere.²²⁻²⁵ Only a brief description is provided here. An excimer laser (Lambda Physik LPX 201) at 248 nm was employed to photolyze H₂O₂ generating OH radicals exclusively.²⁶ The photolysis laser was operated at a repetition rate of 0.3 Hz and laser fluence of ~15 mJ cm⁻². The low pulsing frequency of the excimer laser ensured a complete replenishment of the gaseous mixtures inside the flow reactor before the next photolysis event. For OH excitation, the probe laser beam at 282 nm was produced by frequency doubling of a dye laser (Sirah Laser PrecisionScan PRSC-24-HPR, rhodamine 6G dye), which was pumped by the frequency-doubled output of a Nd:YVO₄ laser (Spectra Physics Navigator II YHP40-532QW). The probe wavelength of 282 nm corresponds to the (1,0) vibrational band of the A-X electronic system of OH radical. The probe laser had an output beam power of ~20 mW at a repetition rate of 10 kHz, providing relative OH profiles with a time resolution of 100 μs. The synchronization of the photolysis beam and probe beam was achieved with the aid of a delay generator (Princeton Research 9650). OH radical decay was monitored by capturing the red-shifted laser-induced fluorescence signal at ~308 nm.

Water-free H₂O₂ was used as an OH radical precursor.²⁷ A variable concentration of water-free H₂O₂ was obtained by adjusting the flow of helium through a flask containing a mixture of urea-H₂O₂ (97%, Sigma Aldrich, m.p = 84-86 °C) powder and SiO₂ at 40 °C. Absolute concentration of HO₂ radicals were measured occasionally by employing continuous wave Cavity Ring Down

Spectroscopy (cw-CRDS) technique in the $2 \nu_1$ transition at 6638.2 cm^{-1} .²⁸ The OH-LIF and HO₂-CRDS signals were fitted simultaneously allowing to retrieve the initial concentration of H₂O₂ and OH concentrations. A typical H₂O₂ $\sim 1 \times 10^{14} \text{ cm}^{-3}$ concentration was obtained *via* the thermal decomposition of the H₂O₂-urea mixture, which yielded an initial concentration of OH radicals of $\sim 3 \times 10^{11} \text{ cm}^{-3}$. Together with the known absorption-cross section of H₂O₂ at 248 nm ($9.37 \times 10^{-20} \text{ cm}^2$), a photolysis energy of $\sim 15 \text{ mJ/cm}^2$ can be calculated, in excellent agreement with measurements. Ball and Massey²⁹ reported that partial decomposition of H₂O₂-urea adduct occurs at temperatures as low as 325 K ($E_a = 113 \text{ kJ/mol}$ and $A = 4.8 \times 10^{13} \text{ s}^{-1}$ for fresh urea-H₂O₂ and $E_a = 66 \text{ kJ/mol}$ and $A = 10^6 \text{ s}^{-1}$ aged urea-H₂O₂). Dilute mixtures of 1,4-CHD in helium were prepared manometrically in glass balloons. The mixture was introduced into the flow reactor by adding a small portion of the mixture to the main flow of helium through calibrated flowmeters. All experiments were carried out in the presence of 1 Torr of O₂ at a total pressure of 49 Torr helium.

3. Computational Methods

Electronic structure calculations for all stationary points were carried out at M06-2X/aug-cc-pVTZ^{30, 31} functionals using Gaussian 09 suite³². Note that M06-2X functional is known to be the best performing functional for obtaining barrier heights for many reaction systems while not raising the computational cost.^{30, 31, 33} This method has also been broadly demonstrated to precisely forecast structures and frequencies^{34, 35}. In particular, M06-2X/aug-cc-pVTZ level of theory has been shown to give reliable results in predicting rate constants for several chemical kinetic investigations of imidazole + OH³⁶, oxazole + OH³⁷, pyrrole + OH³⁸, *trans*-decalin + OH³⁹, and aniline + OH⁴⁰. The same M06-2X/aug-cc-pVTZ level of theory was employed method to

determine the harmonic vibrational frequencies for each stationary point. The zero-point vibrational energy (ZPVE) corrections were obtained with a scaling factor of 0.971⁴¹ for the harmonic vibrational frequencies to correct the gap between the measured and predicted data. Intrinsic reaction coordinate (IRC)^{42, 43} calculations were also done at the M06-2X/aug-cc-pVTZ level of theory to check if a transition state appropriately links with its desirable minima, thus finding the corresponding reactant (**RC**) and product (**PC**) complexes for all reaction pathways. Molecular characteristics (i.e., Cartesian coordinates, rotational constants, electronic energies, harmonic vibrational frequencies, ZPE corrections and optimized structures) for all species on the PES were also obtained at M06-2X/aug-cc-pVTZ level of theory and are compiled in the Supplementary Information (Table S1 and Figure S1).

Comprehensive kinetic analyses (e.g., phenomenological rate coefficients $k(T, P)$ and time-resolved species profiles) were carried out using the Multi-Species Multi-Channel (MSMC) code^{44, 45} with the stochastic^{46, 47} RRKM-ME rate model where corrections for quantum tunneling effect and hindered internal rotation (HIR) treatment were included. A statistically sufficient number of 10^8 trials were taken in stochastic simulations. Eckart⁴⁸ tunneling based on one-dimensional (1D) asymmetrical potential was employed, while the procedure of HIR correction was described in our previous study⁴⁹. The HIR parameters (automatically yielded with the aid of Graphical User Interface^{50, 51}) are given in the Supplementary Information (SI) file.

For master equation calculations, a single exponential down model was employed to characterize the collisional energy transfer with the average downward energy transfer parameter $\langle \Delta E_{\text{down}} \rangle = 260.0(T/298 \text{ K})^{0.8} \text{ cm}^{-1}$ for argon bath gas. Here, the temperature-dependent component was

adopted from Tan *et al.*⁵² and $\langle \Delta E_{\text{down}} \rangle$ value of 260.0 cm⁻¹ at 298 K as suggested by Joshi *et al.*⁵³. Lennard-Jones (L-J) parameters, $\varepsilon / k_B = 113.5$ K and $\sigma = 3.465$ Å, for Ar were taken from Hippler *et al.*⁵⁴, whereas the L-J parameters for the reactant-complex (**RC**) and adduct (**II**) were assumed to be the same as those for phenol⁵⁵ ($\varepsilon / k_B = 600.9$ K and $\sigma = 5.218$ Å). Beyer–Swinehart algorithm⁵⁶ was used for harmonic oscillator (HO) modes to achieve the density/sum of states, which was then convoluted with external/hindered rotational modes using the Fast Fourier Transform (FFT) approach⁵⁷. An energy bin size of 1 cm⁻¹ was applied for the density of state (DOS) computations.

Inverse Laplace Transform (ILT) technique⁵⁸ was employed for the entrance channel, i.e., the barrierless association reaction of 1,4-CHD and OH radicals, forming a pre-reactive complex (RC). For ILT treatment, a temperature-independent value of 4.0×10^{-10} cm³/molecule/s was taken for the high-pressure-limit (HPL) rate constant corresponding to the long-range transition state (LR-TST).⁵⁹ Such a treatment has been found to reliably predict the kinetics of reaction systems that proceed via the formation of pre-reaction complexes, e.g., association reactions of cyclic compounds + OH.³⁶⁻⁴⁰

4. Results and Discussion

4.1 Experimental Rate Coefficients.

Rate coefficients for the reaction of OH radicals with 1,4-CHD were measured at 5 different temperatures over the temperature range of 295 – 436 K. Figure 1(a) shows a typical example of the LIF signal of OH radicals obtained at $T = 436$ K and $P \sim 50$ Torr. Figure 1(a) also displays

OH-LIF signal recorded in a control experiment with H₂O₂ and He only. For each temperature, five different concentrations of 1,4-CHD in the range of 0.46 – 2.18×10¹³ molecules/cm³ were used, whereby two consecutive series of concentration ramps were carried out. The OH decay profiles were fitted to a single exponential decay. As seen, OH decays obeying the first-order kinetics (see also log[OH] versus time plot in Fig. 1(b)). From these plots, pseudo-first-order rate constants (k'_{1st}) were obtained for each 1,4-CHD concentration. As seen in Figure 1(c), k'_{1st} versus 1,4-CHD concentration plot yields a straight line with a slope (k'_{1st}) = k_{bi} [1,4-CHD]. k_{bi} is the bimolecular rate coefficient for the reaction of OH radicals with 1,4-CHD at a given temperature. The linear plot has a non-zero intercept representing the OH radical loss due to its reaction with the precursor H₂O₂ and its diffusion out of the observation volume. Extrapolation of the linear regression to [1,4-CHD] = 0 cm⁻³ was always in good agreement with the measured value (see Table 1).

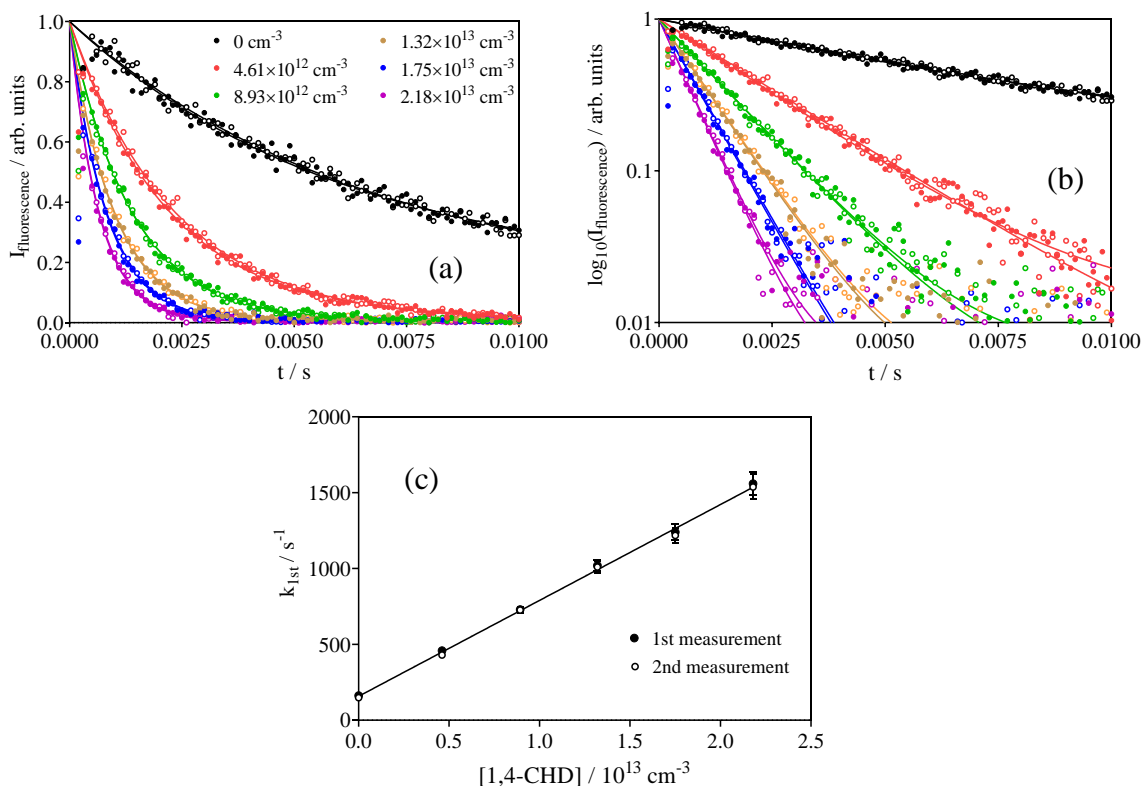


Figure 1. Typical OH decay time profiles measured for 5 different concentrations of 1,4 CHD over $0.46 - 2.18 \times 10^{13}$ molecules/cm³ at $T = 438$ K and $P \sim 50$ Torr. A control experiment for OH decay with H₂O₂ alone is also shown (black symbols). (a) linear y-axis, (b) logarithmic y-axis, (c) plot of k_{1st} as a function of [1,4-CHD]; error bars represent 95% confidence interval obtained from linear regression. Filled and open circles represent the experimental data from the first and second series, respectively.

At 295 K, we determined a rate coefficient of $k(\sim 50 \text{ Torr}) = (9.73 \pm 0.32) \times 10^{-11} \text{ cm}^3/\text{molecule/s}$ which is in excellent agreement with the room-temperature data from Ohta¹⁸ $k(760 \text{ Torr}) = (9.86 \pm 0.31) \times 10^{-11}$ and Atkinson et al.¹⁹ $k(\sim 735 \text{ Torr}) = (9.48 \pm 0.39) \times 10^{-11}$. Using structure-reactivity relationship and linear free-energy relationship, Grosjean et al.⁶⁰ estimated a value of $k(298 \text{ K}, 760 \text{ Torr}) = 7.2 \times 10^{-11} \text{ cm}^3/\text{molecule/s}$ for the rate coefficient of OH radicals with 1,4-CHD. With $k(298 \text{ K}, 760 \text{ Torr}) \sim 10^{-10} \text{ cm}^3/\text{molecule/s}$ and a typical OH atmospheric concentration of $\sim 10^6 \text{ molecules/cm}^3$, the lifetime ($\tau = 1/k[\text{OH}]$) of 1,4-CHD appears to be ~ 2.8 hours. Such a

short lifetime suggests that once 1,4-CHD is released into the atmosphere, it will be quickly oxidized by atmospheric oxidants to form a wide spectrum of highly oxidized organic species. Therefore, OH-initiated oxidation of 1,4-CHD plays a critical role in the atmosphere reactivity affecting the local air quality. The experimental data for the rate coefficients over a wide range of pressures show that the rate coefficients are already close to the high-pressure limit, which is not surprising. With the increase of molecular complexity i.e. no. of vibrational degrees of freedom, the falloff regime shifts significantly towards the lower total pressures according to unimolecular rate theory.

Our measured values of the rate coefficients exhibited a discernible negative temperature dependence (see Fig. 5). The rate coefficients showed an appreciable drop while increasing the temperature from 295 K to 438 K, $k(438 \text{ K}) = (6.32 \pm 0.21) \times 10^{-11} \text{ cm}^3/\text{molecule}/\text{s}$. Note that the reaction of OH radicals with 1,4-CHD exhibits a positive T -dependence at high temperatures.¹⁷ The complex temperature dependence of such a reaction is not surprising considering the competition between OH addition and hydrogen abstraction channels. Moreover, as stated earlier, the transition state corresponding to allylic hydrogen abstraction is submerged below the reactants' energy. Such a negative reaction barrier further adds complexity to this chemical system which warrants a detailed theoretical analysis to fully rationalize the temperature and pressure dependence of the reaction and to discern the role of various competing channels.

Table 1. Temperature dependence of the pseudo-first order rate coefficients $k(T, P \sim 50 \text{ Torr})$ for the reaction of OH radicals with 1,4-cyclohexadiene (1,4-CHD), the overall bimolecular rate coefficients (k_{bi}) (uncertainty is statistical only) and intercept I (extrapolation of linear regression to $[1,4\text{-CHD}] = 0 \text{ cm}^{-3}$)

T / K	$[1,4\text{-CHD}] / 10^{13} \text{ molecules cm}^{-3}$	k'_{1st} / s^{-1}	$k_{\text{bi}} / 10^{-11} \text{ cm}^3 \text{ molecule}^{-1} \text{ s}^{-1}$	I / s^{-1}
295.15	0	258 ± 6.5		
	0.60	898 ± 9		

	1.14	1400 ± 15		
	1.67	1930 ± 34	9.73 ± 0.35	284 ± 53
	2.2	2396 ± 53		
	2.73	2943 ± 104		
322.15	0	193 ± 32		
	0.56	765 ± 16		
	1.05	1212 ± 33		
	1.54	1696 ± 47	9.1 ± 0.59	236 ± 91
	2.02	2036 ± 138		
	2.51	2504 ± 153		
372.15	0	251 ± 18		
	0.50	509 ± 88		
	0.95	959 ± 207		
	1.40	1297 ± 242	7.74 ± 1.33	219 ± 120
	1.85	1659 ± 322		
	2.30	1763 ± 564		
399.15	0	172 ± 78		
	0.51	552 ± 32		
	0.98	1005 ± 37		
	1.45	1319 ± 40	7.36 ± 0.4	221 ± 58
	1.92	1657 ± 39		
	2.39	1894 ± 69		
438.15	0	162 ± 22		
	0.46	458 ± 15		
	0.89	729 ± 23	6.32 ± 0.20	157 ± 26
	1.32	1020 ± 37		
	1.75	1240 ± 55		
	2.18	1559 ± 78		

4.2 Potential Energy Surface (PES)

Figure 2 presents ZPE-corrected energy profile (0 K), obtained at M06-2X/aug-cc-pVTZ level of theory, for OH + 1,4-CHD reaction. For convenience, energies relative to that of the separated reactants are taken for discussion unless otherwise stated. Similar to OH + alkenes^{21, 61, 62}, the interaction between an OH radical and 1,4-CHD can yield a pre-active vdW complex (or the so-called reactant-complex, **RC**) as an initial step (see Figure 2), which typically occurs without an

intrinsic barrier. The well-depth of **RC** is located at -4.8 kcal/mol, which is significantly deeper than that of ethylene + OH⁶¹ (-1.9 kcal/mol), propene + OH^{21, 63} (-2.2 kcal/mol), 1-butene + OH⁶² (-3.0 kcal/mol) and benzene + OH⁶⁴ (-2.8 kcal/mol). Similar stabilization energy of **RC** was seen in toluene + OH³³ (-4.8 kcal/mol), but it is somewhat smaller than that of hexamethylbenzene (HMB) + OH⁶⁵ (-6.5 kcal/mol). The extra stabilization of **RC** in HMB + OH reaction appears to stem from the six electron-donating methyl groups.

From the initially-formed **RC**, OH radicals could either add to C=C bonds or abstract an H atom from an allylic site (C_β-H) through the submerged transition states, **TS1** (-2.9 kcal/mol) and **TS4** (-1.4 kcal/mol), respectively. The submerged **TS** for OH addition to the double bond of 1,4-CHD is not surprising as negative barrier heights have been reported for other alkenes + OH reactions^{21,62}. However, it is not a common occurrence for hydrogen abstraction reactions. Nonetheless, there are some reports of negative energy barriers for hydrogen abstraction reactions as well, e.g., hepta-2,5-dienes + OH⁶⁶ (-1.1 and -3.4 kcal/mol for monoallylic and bisallylic hydrogen abstraction, respectively), toluene + OH³³ (-0.5 kcal/mol) and HMB + OH⁶⁵ (-1.1 kcal/mol) for hydrogen abstraction from the CH₃-site. Here, both the addition and abstraction reactions originate from the same complex **RC**, which was confirmed by the IRC calculations. The former leads to the formation of the adduct, **I1**, with an exothermicity of -29.5 kcal/mol. The chemically activated adduct, **I1**, can undergo β-scission reactions by breaking either C_α-H or C_β'-H bonds through **TS2** (2.5 kcal/mol) and **TS3** (6.4 kcal/mol), respectively, leading to bimolecular products, **P1** + H (-3.2 kcal/mol) and **P2** + H (2.2 kcal/mol) (see Figure 2). Hydrogen abstraction channel proceeds via **TS4** leading to the formation of product-complex **PC1** (-46.4 kcal/mol), which promptly dissociates to the final products, **P3** + H₂O, in a relatively high overall exothermicity of 42.4 kcal/mol. Furthermore, direct H-abstraction channel from vinylic C_α-H

bonds of 1,4-CHD by OH radical can proceed through **TS5** (2.1 kcal/mol), resulting in the formation of product-complex **PC2** (-11.8 kcal/mol), which immediately dissociates to the exit channel, **P4** + H₂O (-9.3 kcal/mol).

It is worth mentioning that the two product-complexes, **PC1** & **PC2**, sit at considerably lower energies than their corresponding **TSs** (i.e., ~ 45.0 and 13.9 kcal/mol lower than **TS4** and **TS5**, respectively). Thereby, it is expected that the energized complexes are unfavorably stabilized (except in the case of extremely high pressures) but directly yield the final products, **P3** + H₂O and **P4** + H₂O, with the low threshold energies of 4.0 and 2.5 kcal/mol, respectively. These **PCs**, therefore, can be reasonably neglected in kinetic simulations since the decomposition of the **PCs** is not the rate-determining species.^{38, 67} For the current chemical system, the accuracy of the predicted rate coefficients relies heavily on precisely locating the relative position of the inner transition states. Therefore, the main channels leading via **TS1**, **TS4** and **TS5** (**TS1** and **TS4** dictate the low-*T* kinetics, see sections 4.3 and 4.4) were also calculated at a higher level of theory, i.e., CCSD(T)/CBS//M06-2X/aug-cc-pVTZ⁶⁸⁻⁷⁰, using two basis sets of cc-pVTZ and cc-pVQZ and then extrapolating to the complete basis set (CBS) by applying Halkier's scheme.⁷¹ The results are compared in Table S7 of SI. As seen, a good agreement between the two ab initio approaches was obtained, e.g., -2.9 vs. -2.6 kcal/mol and -1.4 vs. -0.9 kcal/mol for **TS1** and **TS4**, at M06-2X/aug-cc-pVTZ and CCSD(T)/CBS//M06-2X/aug-cc-pVTZ levels of theory, respectively. The maximum deviation of ~ 0.7 kcal/mol was observed for **TS5**, and it is within the quantum methods' chemical accuracy (~1 kcal/mol). Both methods employed here yielded a very comparable rate coefficients (see Fig. S6 of SI). The rate coefficients obtained using the PES from the M06-2X/aug-cc-pVTZ level of theory are about ~ 1.4 times faster than from CCSD(T)/CBS//M06-2X/aug-cc-pVTZ level of theory. Interestingly, the PES at the M06-2X/aug-cc-pVTZ level of theory yielded

the rate coefficients that agree remarkably with the experimental data (see section 4.5). Thus, we consider M06-2X/aug-cc-pVTZ as an appropriate method to characterize the kinetic behavior of 1,4CHD + OH reaction.

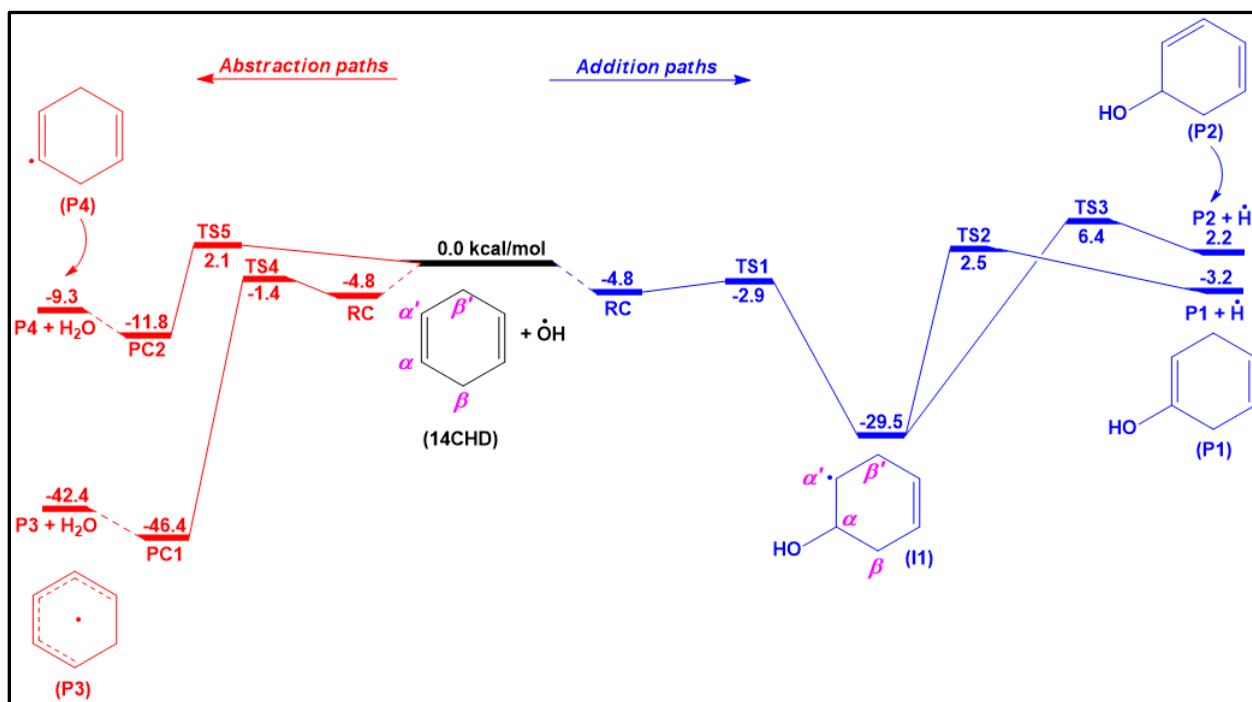


Figure 2. ZPE-corrected energy profile (0 K) for 1,4-CHD + OH reaction calculated at the M06-2X/aug-cc-pVTZ level of theory. Energy values are given in kcal/mol.

4.3 Kinetic Model

It is well-known that OH initiated oxidation of unsaturated organic compounds proceeds via a complex-forming mechanism. For such chemical systems, OH first adds to the unsaturated bond of the organic molecule forming a pre-reactive complex (denoted as RC for 1,4CHD+OH reaction system) through a barrierless process (outer transition state). The RC then dissociates to form intermediate(s)/products (here, **I1** or **P3** + H₂O, see Fig. 2) via well-defined transition states (inner transition states). Klippenstein and co-workers, through the study of OH reactions with C₂H₄⁷² and isoprene^{72, 73}, demonstrated that the kinetics of such chemical systems could be treated accurately

using a two-transition state (2-TS) model. The authors indicated that the outer transition state governs kinetics at ultracold temperatures relevant to interstellar atmospheres. However, at high temperatures ($T > 200$ K), the reaction kinetics of such chemical systems are pretty much governed by the inner transition state, and the 2-TS model can overestimate the rate coefficients (see also Georgievskii and Klippenstein⁷⁴). Therefore, instead of coupling the inner and outer transition states as in Klippenstein and co-workers' 2-TS model, we explicitly considered the two transition states into the reaction network (i.e., $\text{CHD} + \text{OH} \rightarrow [\text{outer transition state}] \rightarrow \mathbf{RC} \rightarrow [\text{inner transition states: } \mathbf{TS1/TS4}] \rightarrow \mathbf{I1/(P3 + H_2O)}$) within the ME framework. As stated earlier, for the barrierless process (i.e., $\text{CHD} + \text{OH} \rightarrow [\text{outer TS}] \rightarrow \mathbf{RC}$), the microscopic rate constant $k(E)$ were calculated by employing the Inverse Laplace Transform (ILT) technique⁵⁸, which used a temperature-independent value of $k^\infty(T)$ of 4.0×10^{-10} cm³/molecule/s, based on LR-TST treatment⁵⁹.

To identify the role of the outer TS, we carried out the sensitivity of the assigned $k^\infty(T)$ for the barrierless association process on the predicted values of $k(T, P)$. For the sensitivity analysis, $k^\infty(T)$ was changed from 4.0×10^{-10} to 4.0×10^{-11} and 4.0×10^{-9} cm³/molecule/s (uncertainty of a factor of 10). Such a significant change in $k^\infty(T)$ led to a decrease/increase in the total rate coefficients by a factor of 6.2/2.4, 3.8/1.9, and 1.1/1.2 at $T = 200$ K, 300 K, and 1000 K and $P = 760$ Torr, respectively. As expected, the outer-TS only plays a role at low temperatures. Incorporation of such a significant uncertainty for the entrance channel does not essentially deteriorate the predicted values of the rate coefficients above 300 K, indicating that RC has no significant kinetic relevance at high temperatures (see Figure S7). As for the inner-TSs, we performed the variational transition theory to evaluate the variational effects of two critical channels via transition states **TS1** and **TS4** (i.e., $\mathbf{RC} \rightarrow [\mathbf{TS1}]^\ddagger \rightarrow \mathbf{IM1}$ and $\mathbf{RC} \rightarrow [\mathbf{TS4}]^\ddagger \rightarrow \mathbf{P3} + \text{H}_2\text{O}$). The minimum energy pathways

(MEP) are shown in Figure S8. We found that the variational effect (described by the ratios of $k_{\text{TST}}(T)$ to $k_{\text{VTST}}(T)$ as in Table S8) is not necessary for an accurate kinetic picture for both channels taking place via TS1 and TS4 over the temperature range of 200 – 2000 K. As seen in Table S8, the variational effect caused the rate coefficients to drop by a factor less than 2. Thus, the variational effect is not included in the master equation model to simplify the simulations without compromising the model's prediction.

4.4 Simulated Time-resolved Species Profiles

In order to characterize the kinetic behavior of 1,4-CHD + OH reaction, a stochastic RRKM-ME model was applied over $T = 200 - 2000$ K and $P = 0.76 - 7600$ Torr in Ar bath gas using the molecular parameters and energy profile from M06-2X/aug-cc-pVTZ level of theory. These calculations included the corrections for hindered internal rotations (HIR) and tunneling effects. Using the PES displayed in Figure 2, the normalized time-resolved profiles of the species involved in the reaction were computed (see Figure 3). For these calculations, **PC1** & **PC2** were excluded for the reasons discussed in the previous section. At 298 K and 760 Torr, a small portion of **RC** appears very briefly at short time scales, so we can conclude that **RC** has no kinetic relevance. At $t \leq 1.38 \times 10^6$ s, the stabilization of the adduct, **I1**, prevails over the product channel, **P3** + H₂O, e.g., consuming ~ 53.0% and 46.6% of the reactants, respectively. At $t = 10^6$ s, the formation of **P3** + H₂O is exclusive while **P4** + H₂O only takes ~ 0.3%. At atmospheric conditions, the other products are kinetically insignificant (e.g., more than four orders of magnitudes lower than **P3** + H₂O). At $t > 1.38 \times 10^6$ s, the product channel, **P3** + H₂O, accounts for ~ 99.5% of the consumption of reactants.

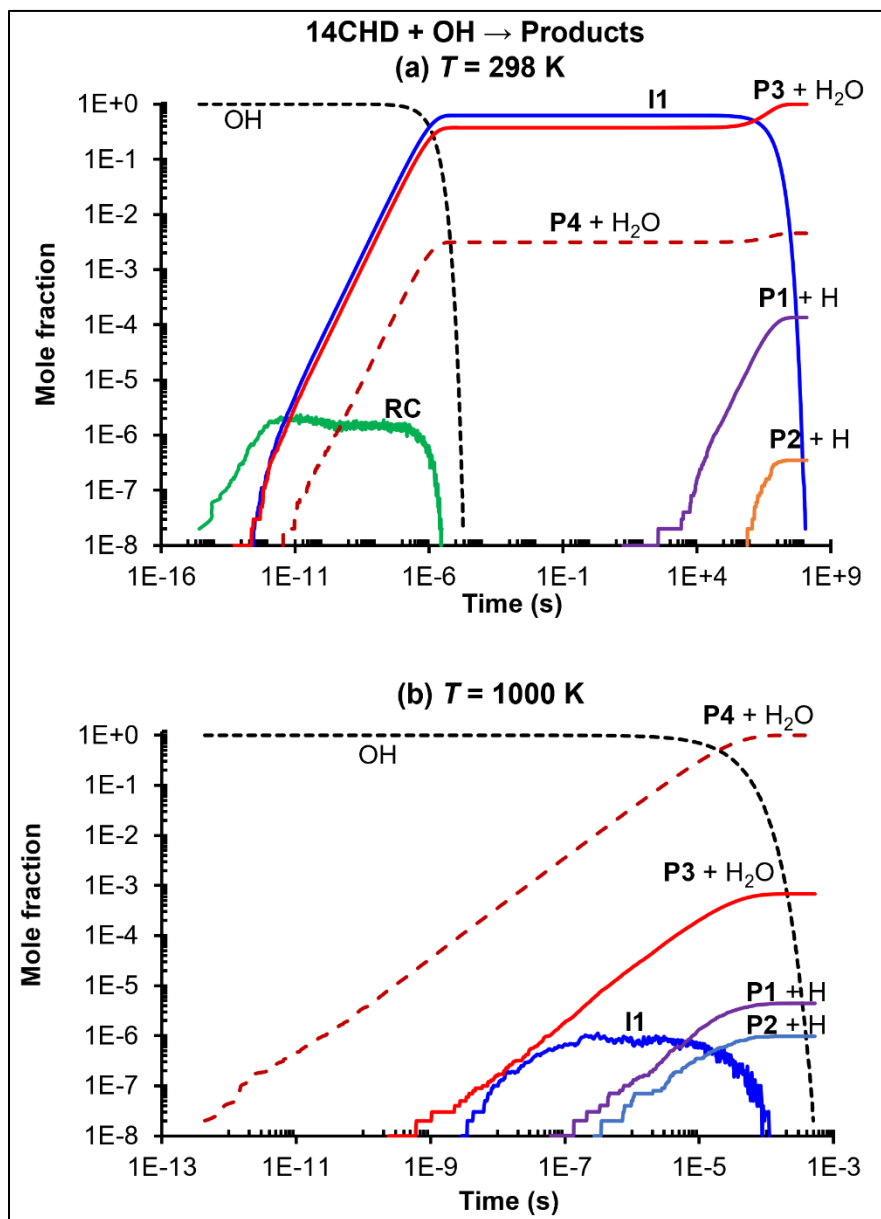


Figure 3. Computed time-resolved species profiles for the reaction of $1,4\text{-CHD} + \text{OH} \rightarrow \text{products}$, at 298 K (a) and 1000 K (b) using the stochastic (with 10^8 numbers of trials) approach with $[1,4\text{-CHD}]/[\text{Ar}] = 3 \times 10^{-4}$ and $[1,4\text{-CHD}]_0 \gg [\text{OH}]_0$. Kinetic simulations were carried out using the full PES (excluding the PCs) depicted in Figure 2.

At 1000 K and 760 Torr (see Fig. 3(b)), **RC** has completely disappeared as expected. Unlike the kinetic picture at 298 K, the adduct, **I1**, appeared in a very small fraction revealing a negligible kinetic relevance. Similarly, the bimolecular products, **P1** + H and **P2** + H, are of negligible importance. At all reaction times, the hydrogen abstraction channel, **P4** + H₂O, dominates while **P3** + H₂O has a minor contribution to the consumption of reactants. This kinetic picture remains unchanged for temperatures above 1000 K and pressure of 760 Torr.

4.5 Theoretical Rate Coefficients $k(T, P)$

The phenomenological rate constants, $k(T, P)$, for each channel of the reaction, 1,4-CHD + OH \rightarrow intermediates/products, are plotted in Figure 4 as a function of temperature at $P = 760$ Torr, and are summarized in Table S5. At $T \leq 500$ K, the stabilization of the adduct **I1** dominates the formation of **P3** + H₂O, and k_{11} declines with increasing temperatures. This is expected as the exit barriers for the reactions of **I1** are higher than the reactants' energy and the reverse barrier is submerged below the reactants. Consequently, the adduct dissociates back to the reactants at higher temperatures. Similar observations have previously been made for pyrrole + OH³⁸. Such kinetic behaviour may indicate the existence of submerged barrier heights and pre-active vdW complex.⁷⁵ Unlike the other alkenes + OH reactions, hydrogen abstraction channel of 1,4-CHD + OH was found to contribute significantly at lower temperatures, e.g., ~35% at 200 K and ~44% at 500 K. However, this is not too surprising in view of the salient features of the PES of 1,4-CHD + OH reaction. As discussed earlier, the abstraction of an H atom from allylic C _{β} -H occurs through the submerged transition state. Due to the negative barrier height, the C _{β} -H hydrogen abstraction

reaction displayed an unusual negative temperature dependence (see Fig. 4). Similar peculiarities have previously been observed for hydrogen abstraction reaction of acetaldehyde (CH_3CHO) with OH radicals (see D'Anna et al.⁷⁶). Since the addition reaction had no kinetic relevance under atmospheric conditions, D'Anna et al.⁷⁶ reported a strong negative temperature dependence for hydrogen abstraction reaction of $\text{OH} + \text{CH}_3\text{CHO}$ at low temperatures as a result of the submerged transition state and the existence of pre-reaction complexes.

Clearly, the hydrogen abstraction channel, $\text{P3} + \text{H}_2\text{O}$, competes with the addition channel forming **II** at lower temperatures. At $T \sim 600$ K, the reactants proceed via these two channels with nearly equal rates ($\sim 6 \times 10^{-12}$ $\text{cm}^3/\text{molecule/s}$ at 760 Torr). At $T \geq 700$ K, the production of $\text{P4} + \text{H}_2\text{O}$ is dominant. The predicted pressure- and temperature-dependence of the rate constant, $k_{\text{II}}(T, P)$, leading to the stabilization of the adduct **II**, is plotted in Figure S2 (Supplementary Information). As expected, $k_{\text{II}}(T, P)$ displays a negative temperature dependence and a strong positive pressure dependence in the intermediate temperature regime. Our calculated value of the rate coefficient, $k_{\text{II}}(298 \text{ K}, 760 \text{ Torr}) = 7.5 \times 10^{-11}$ $\text{cm}^3/\text{molecule/s}$, shows a good agreement with the structure-activity relationship (SAR) predicted value of 1.2×10^{-10} $\text{cm}^3/\text{molecule/s}$ from Peeters *et al.*⁷⁷

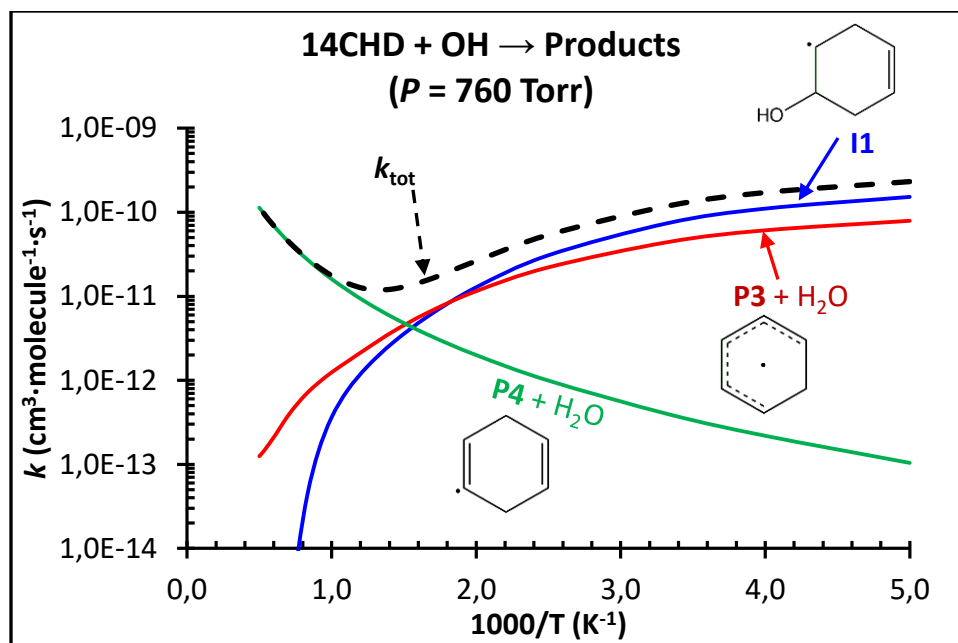


Figure 4. Predicted rate coefficients for the reaction, 1,4-CHD + OH \rightarrow intermediates/products reaction as a function of temperature at $P = 760$ Torr. The observed U-shaped Arrhenius curve of the global rate constants reflects the salient features of the PES, revealing channel switching from low temperature (**I1** + H₂O and **P3** + H₂O channels) to high temperature (**P4** + H₂O channel).

Figure 5 presents total rate coefficients, $k_{\text{tot}}(T, P)$, as a function of temperature at $P = 760$ Torr and compares with experimental¹⁷⁻¹⁹ and theoretical⁷⁸ works to gauge the reliability of our RRKM-ME calculations. Rate coefficients, $k_{\text{tot}}(T, P)$, at different pressures ($P = 0.76 - 7600$ Torr) are shown in Figure S3 and compiled in Table S3. Figure S4 presents the role of the hindered rotor treatment to accurately compute the rate coefficient for the current chemical system. Double Arrhenius parameters from the best fit of the computed $k_{\text{tot}}(T, P)$ are listed in Table 2. As seen in Figure 5, our computed value of rate coefficient, $k_{\text{tot}}(300 \text{ K}, 760 \text{ Torr}) = 1.19 \times 10^{-10} \text{ cm}^3/\text{molecule/s}$, is in good agreement with our experimental data $k(295 \text{ K}, 50 \text{ Torr}) = 9.73 \times 10^{-11}$ as well as literature data of Ohta¹⁸ $k(297 \text{ K}, 760 \text{ Torr}) = 9.86 \times 10^{-11}$ and Atkinson *et al.*¹⁹ $k(298 \text{ K}, 760 \text{ Torr}) = 9.48$

$\times 10^{-11}$. Our calculated rate coefficient is slightly higher than the SAR predicated value (7.2×10^{-11}) of Grosjean *et al.* (1992)⁷⁸.

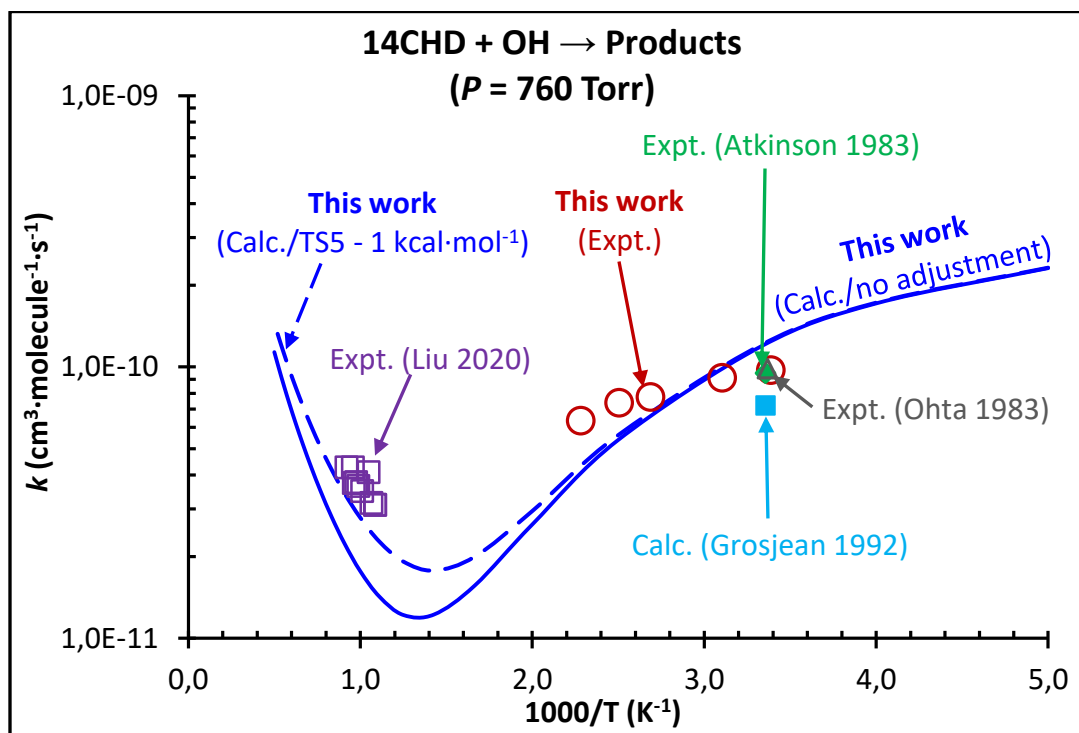


Figure 5. Comparison between the calculated and experimental global rate coefficients, $k(T, P)$, for 1,4-CHD + OH \rightarrow Products. Literature data are from the works of Liu *et al.*¹⁷ (“Exp. (Liu 2020)”), Grosjean *et al.*⁷⁸ (“Calc. (Grosjean 1992)”), Ohta¹⁸ (“Exp. (Ohta 1983)”) and Atkinson *et al.*¹⁹ (“Exp. (Atkinson 1983)”).

Our calculated values of rate coefficients exhibit no discernible pressure dependence which goes in line with our earlier notion that our measured experimental rate coefficient at 50 Torr is already close to the high-pressure limit. As seen, our calculations nicely capture the experimental trend of the rate coefficients, displaying a weak negative temperature in the low-temperature regime (see Fig. 5). At high temperatures, our calculated values of global $k_{\text{tot}}(T, P)$ is lower by a factor of ~ 2 than our earlier shock tube measurement¹⁷, e.g., 2.2×10^{-11} vs. 4.3×10^{-11} $\text{cm}^3/\text{molecule/s}$ at $T \sim 1089$ K. With a lowering of the barrier height of **TS5** by 1 kcal/mol, our theoretical rate coefficients

follow the trend of the temperature dependence of the experimental rate coefficients very well. It is worth noting that both HIR and tunneling treatments have a minor effect on the theoretical rate coefficients. For instance, HIR correction speeds up the global rate constants at 760 Torr by a factor of ~ 1.2 , 1.8 and 1.6 at $T = 200$ K, 1000 K and 2000 K, respectively (see Figure S4). Similarly, Eckart quantum tunneling increases the rate coefficients at 300 K by a factor of 1.1, 1.6 and 1.9 for the main channels **I1**, **P3 + H₂O** and **P4 + H₂O**, respectively. Nonetheless, tunneling corrections are needed to account for reliable rate coefficients at low temperatures ($T \leq 500$ K, see Table S4).

We observed that the reaction of OH radicals with 1,4-CHD displays a complex kinetic behavior yielding a U-shaped Arrhenius behavior which is known to be a peculiar characteristic of alkene + OH reactions. However, we observed some unusual features in the reaction of OH radicals with 1,4-CHD + OH, e.g., (i) negative temperature dependence of the abstraction reaction owing to the negative barrier height of this chemical pathway, (ii) a significant contribution of the abstraction channel, as large as $\sim 35\%$, under atmospheric conditions which contradicts the conventional understanding of alkenes + OH reactions. For other alkenes, the reactions are known to exclusively undergo via the addition of OH radical to the double bond under atmospheric conditions. Our findings for the reaction of OH radicals with 1,4-CHD are crucial to understanding the OH-initiated oxidation kinetics of cyclic and acyclic dienes.

Table 2: Temperature and pressure dependence of the total rate coefficients $k(T, P)$, fitted to double modified Arrhenius parameters, as given by $k(T) = A_1 T^{n_1} \exp(-E_1 / T) + A_2 T^{n_2} \exp(-E_2 / T)$ in units of $\text{cm}^3 \text{ molecule}^{-1} \text{ s}^{-1}$ for $T = 200 - 2000$ K.

P (Torr)	A_1 ($\text{cm}^3 \text{ molecule}^{-1} \text{ s}^{-1}$)	n_1	E_1 (K)	A_2 ($\text{cm}^3 \text{ molecule}^{-1} \text{ s}^{-1}$)	n_2	E_2 (K)	Fitting error % in $k(T)$
0.76	3.58×10^5	-5.67	986.0	3.35×10^{-18}	2.33	705.2	0.4
7.6	2.93×10^5	-5.64	977.2	2.77×10^{-19}	2.63	254.8	0.3

76.0	3.52×10^5	-5.67	983.8	1.71×10^{-19}	2.68	155.6	0.2
760.0	2.73×10^5	-5.63	971.4	3.68×10^{-19}	2.59	267.4	0.2
7600.0	4.59×10^8	-5.72	971.6	1.41×10^{-19}	2.70	92.1	0.3

4.6 Branching Ratios

Figure 6 shows predicted branching ratios of various channels as a function of temperature at $P = 760$ Torr. The stabilization of **I1** is dominant below 500 K, and the hydrogen abstraction channel, **P3** + H₂O, contributes significantly at low temperatures. At 500 K and 760 Torr, branching ratios for **I1**, **P3** + H₂O and **P4** + H₂O are 48.6%, 43.8% and 7.6%, respectively. At high temperatures, the direct hydrogen abstraction channel (**P4** + H₂O) via **TS5** dominates, accounting for ~ 67.9% at 800 K and ~ 90.9% at 1000 K. This channel plays a paramount role at $T \geq 700$ K (see Figure 6).

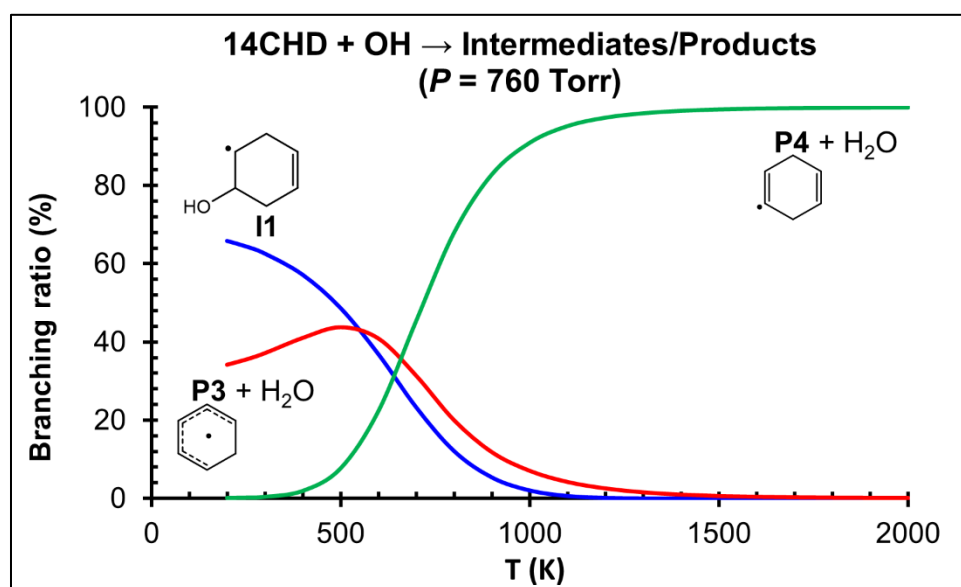


Figure 6. Predicted branching ratios as a function of temperature for 1,4-CHD + OH reaction. The branching ratio is defined as $\Gamma_{X_i}(\%) = \frac{k_{X_i R}}{\sum_{i=1}^{n_X} k_{X_i R}} \times 100$, where $k_{X_i R}$ is the rate constant from the reactants R to species X_i and n_X is the number of species (including intermediates and products).

Reaction flux analyses were carried out at temperatures of 298 K and 1000 K to gain mechanistic insights into the evolution of the chemical system. The results are presented in Figure 7 (see Figure 3a-b for the corresponding species profiles at the two conditions). At the low temperature (298 K), there are two main reaction time scales. At early reaction time ($t \sim 10^{-6}$ s), the main reaction fluxes are the conversion of the reactants to intermediate **I1** and product **P3** + H₂O, accounting for ~ 63.1% and 38.3% of OH conversion, respectively. As time elapses, more **I1** gets formed and attains a quasi-equilibrium until it reaches a large reaction time scale. At $t = 10^6$ s, **I1** starts to deplete to form the product **P3** + H₂O (50%) and the reactants (50%), which in turn react to produce **I1** (58.6%) and **P3** + H₂O (41%). **P3** is formed at two different time scales: (i) “prompt” formation directly from the reactants at the early stage of the reaction, and (ii) “delayed” formation from **I1** and reactants at the late reaction time. At the high temperature (1000 K), the reaction proceeds exclusively (~99.9%) via H-abstraction, forming **P4** + H₂O. Therefore, our analysis of the reaction flux illustrates how the relative importance of the reaction pathways varies with the change of temperature and reaction times.

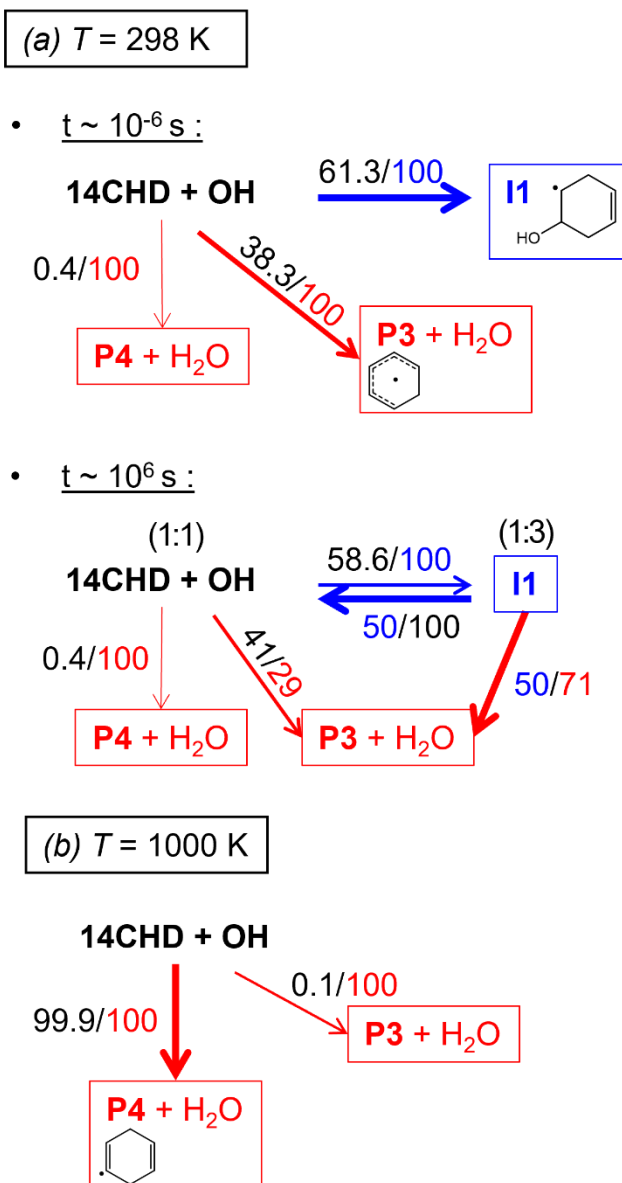


Figure 7. Reaction flux analysis for 1,4-CHD + OH reaction at 760 Torr and (a) 298 K (b) 1000 K. The notation “ r/p ” for a given reaction, reactant(s) \rightarrow product(s), indicates that $r\%$ of the reactant(s) produces $p\%$ of the product(s) in the rate-of-production (ROP) analysis. Here, r and p in are calculated as $r(\%) = \frac{k_{P_i R_j} [R_j]}{\sum_{i=1}^{n_P} k_{P_i R_j} [R_j]} \times 100$ & $p(\%) = \frac{k_{P_i R_j} [R_j]}{\sum_{j=1}^{n_R} k_{P_i R_j} [R_j]} \times 100$, where $k_{P_i R_j}$ is the rate constant from reactant (R_j) to product (P_i); $[R_j]$ is the concentration of R_j ; n_P is the total number of products from R_j , and n_R is the total number of reactants producing P_i . For the reactants and intermediate **I1**, the associating notation ($f:c$) indicates the ratio of the species formation and consumption fluxes as “Formation flux: Consumption flux”. Note that some minor species and insignificant fluxes are not provided for the simplification of the flux network.

5. Conclusions

The kinetics of OH-initiated oxidation reaction of 1,4-CHD was investigated experimentally and theoretically. Experiments were carried out in a flow reactor using laser flash photolysis and laser-induced fluorescence over the temperature range of 295 – 438 K and pressure of ~50 Torr. The Reaction pathways were explored by employing M06-2X/aug-cc-pVTZ level of theory, and RRKM-based master equation calculations were performed to obtain rate coefficients of various channels over 200 – 2000 K and 0.76 – 7600 Torr. Excellent agreement was observed between the theoretical and experimentally determined rate coefficients. Main findings of the current study are summarized below:

- (i) Measured rate coefficients exhibited a negative temperature dependence. Our room temperature value of the rate coefficient showed an excellent agreement with the available experimental data in the literature. By combining our data with the literature data, one can conclude that our measured rate coefficient $k(295 \text{ K}, \sim 50 \text{ Torr}) = 9.73 \times 10^{-11} \text{ cm}^3/\text{molecule/s}$ is close to the high-pressure limit.
- (ii) OH reaction with 1,4-CHD leads to the formation of a pre-reaction complex (**RC**) with a stabilization energy of 4.8 kcal/mol. The stabilization energy of **RC** was found to be significantly higher than that observed for other alkenes + OH reactions. **RC** has a brief lifetime, and the stabilization of **RC** is extremely difficult, even at very high pressures. However, its relative position alters the effective barrier height of the inner transition state, influencing the tunneling correction at low temperatures. Therefore, its inclusion in the kinetic model is inevitable.

- (iii) Like other alkenes + OH reactions, the title reaction was found to display complex kinetics, yielding a U-shaped Arrhenius behavior. Our theoretical kinetic model accurately captured the complex $k(T, P)$ shown by experimental data.
- (iv) Hindered internal rotor and tunneling corrections have a minor effect on the predicted values of the rate coefficients above 300 K.
- (v) The adduct formation channel, II, shows a negative temperature dependence. This adduct forming channel exhibits pressure dependence for $T > 500$ K. However, the total theoretical rate coefficients showed no discernible pressure dependence over $T = 200 - 2000$ K and $P = 0.76 - 7600$ Torr.
- (vi) Some unusual features observed in the reaction of OH radicals with 1,4-CHD + OH are:
 - (a) the transition state corresponding to hydrogen abstraction reaction of 1,4-CHD from the allylic site is significantly submerged below the reactants' energy. As a result, this channel exhibited a negative temperature dependence.
 - (b) the abstraction channel contributes as large as ~35% under atmospheric conditions. This finding contradicts the conventional knowledge of alkenes + OH reactions, which are known to undergo exclusively via the addition of OH radical to the double bond under atmospheric conditions. The findings of this work provide deeper insights into the OH-initiated oxidation kinetics of cyclic and acyclic dienes.

6. Acknowledgments

Research reported in this publication was supported by the Office of Sponsored Research at King Abdullah University of Science and Technology (KAUST). Experiments in Lille were supported by the French ANR agency under contract No. ANR-11-Labx-0005-01 CaPPA (Chemical and Physical Properties of the Atmosphere). This work has received financial support from Institute for Computational Science and Technology (ICST) – Ho Chi Minh City (Grant No. 454/QĐ-KHCNTT) and the Department of Science and Technology (DOST) – Ho Chi Minh City. TVTM was funded by Vingroup Joint Stock Company and supported by the Domestic Master/Ph.D. Scholarship Programme of Vingroup Innovation Foundation (VINIF), Vingroup Big Data Institute (VINBIGDATA) (VINIF.2020.TS.96). C. F. and M. Sz. acknowledge financial support from Hungarian-French BALATON program (TÉT No. 2021-1.2.4-TÉT-2021-00016 / PHC No. 48235NE). Further support was also provided by the National Research, Development, and Innovation Fund (Hungary) within the TKP2021-NVA-14 project.

References

1. H. Richter and J. B. Howard, *Prog. Energy Combust. Sci.*, 2000, **26**, 565-608.
2. N. Hansen, T. A. Cool, P. R. Westmoreland and K. Kohse-Höinghaus, *Prog. Energy Combust. Sci.*, 2009, **35**, 168-191.
3. M. Frenklach, *Phy. Chem. Chem. Phys.*, 2002, **4**, 2028-2037.
4. E. Reizer, I. G. Csizmadia, K. Nehéz, B. Viskolcz and B. Fiser, *Chem. Phys. Lett.*, 2021, **772**, 138564.
5. E. Reizer, I. G. Csizmadia, Á. B. Palotás, B. Viskolcz and B. Fiser, *Molecules*, 2019, **24**, 1040.
6. D. S. N. Parker, F. Zhang, Y. S. Kim, R. I. Kaiser, A. Landera, V. V. Kislov, A. M. Mebel and A. G. G. M. Tielens, *Proc. Natl. Acad. Sci.*, 2012, **109**, 53-58.
7. L. Zhao, M. B. Prendergast, R. I. Kaiser, B. Xu, U. Ablikim, M. Ahmed, B. J. Sun, Y. L. Chen, A. H. Chang and R. K. Mohamed, *Angew. Chem.*, 2019, **131**, 17603-17611.
8. T. Bentz, B. R. Giri, H. Hippler, M. Olzmann, F. Striebel and M. Szöri, *J. Phys. Chem. A*, 2007, **111**, 3812-3818.
9. Z. Wang, L. Ye, W. Yuan, L. Zhang, Y. Wang, Z. Cheng, F. Zhang and F. Qi, *Combust. Flame*, 2014, **161**, 84-100.
10. J. Wang, W. Sun, G. Wang, X. Fan, Y.-Y. Lee, C. K. Law, F. Qi and B. Yang, *Proc. Combust. Inst.*, 2019, **37**, 1091-1098.

11. W. Li, M. E. Law, P. R. Westmoreland, T. Kasper, N. Hansen and K. Kohse-Höinghaus, *Combust. Flame*, 2011, **158**, 2077-2089.
12. N. Hansen, T. Kasper, B. Yang, T. A. Cool, W. Li, P. R. Westmoreland, P. Oßwald and K. Kohse-Höinghaus, *Proc. Combust. Inst.*, 2011, **33**, 585-592.
13. S. S. Nagaraja, G. Kukkadapu, S. Panigrahy, J. Liang, H. Lu, W. J. Pitz and H. J. Curran, *Int. J. Chem. Kinet.*, 2020, **52**, 964-978.
14. D. Smith, P. Cheng and P. Španěl, *Rapid Commun. Mass Spectrom.*, 2002, **16**, 1124-1134.
15. C. A. Taatjes, N. Hansen, A. McIlroy, J. A. Miller, J. P. Senosiain, S. J. Klippenstein, F. Qi, L. Sheng, Y. Zhang and T. A. Cool, *Science*, 2005, **308**, 1887-1889.
16. A. Archibald, M. McGillen, C. Taatjes, C. Percival and D. Shallcross, *Geophys. Res. Lett.*, 2007, **34**, L21801: 21801-L21801: 21804.
17. D. Liu, B. R. Giri, M. Szóri, B. Viskolcz, L. K. Huynh and A. Farooq, *Proc. Combust. Inst.*, 2020, **38**, 947-955.
18. T. Ohta, *J. Phys. Chem.*, 1983, **87**, 1209-1213.
19. R. Atkinson, S. M. Aschmann and W. P. L. Carter, *Int. J. Chem. Kin.*, 1983, **15**, 1161-1177.
20. J. P. Senosiain, S. J. Klippenstein and J. A. Miller, *J. Phys. Chem. A*, 2006, **110**, 6960-6970.
21. J. Zador, A. W. Jasper and J. A. Miller, *Phys. Chem. Chem. Phys.*, 2009, **11**, 11040-11053.
22. A. Parker, C. Jain, C. Schoemaeker and C. Fittschen, *React. Kinet. Catal. Lett.*, 2009, **96**, 291-297.
23. F. Khaled, B. R. Giri, D. Liu, E. Assaf, C. Fittschen and A. Farooq, *J. Phys. Chem. A*, 2019, **123**, 2261-2271.
24. D. Liu, F. Khaled, B. R. Giri, E. Assaf, C. Fittschen and A. Farooq, *J. Phys. Chem. A*, 2017, **121**, 927-937.
25. A. Parker, C. Jain, C. Schoemaeker, P. Szriftgiser, O. Votava and C. Fittschen, *Appl. Phys. B*, 2011, **103**, 725-733.
26. J. Thiebaud, A. Aluculesei and C. Fittschen, *J. Chem. Phys.*, 2007, **126**, 186101.
27. E. Assaf and C. Fittschen, *J. Phys. Chem. A*, 2016, **120**, 7051-7059.
28. J. Thiebaud, S. Crunaire and C. Fittschen, *J. Phys. Chem. A*, 2007, **111**, 6959-6966.
29. M. C. Ball and S. Massey, *Thermochimica acta*, 1995, **261**, 95-106.
30. Y. Zhao and D. G. Truhlar, *Acc. Chem. Res.*, 2008, **41**, 157-167.
31. Y. Zhao and D. G. Truhlar, *Theor. Chem. Acc.*, 2007, **120**, 215-241.
32. M. J. Frisch, G. W. Trucks, H. B. Schlegel, G. E. Scuseria, M. A. Robb et al., Gaussian Inc., 2009.
33. R. M. Zhang, D. G. Truhlar and X. Xu, *Research*, 2019, **2019**.
34. R. K. Robinson and R. P. Lindstedt, *Combust. Flame*, 2013, **160**, 2642-2653.
35. G. Yin, E. Hu, M. Zhou, H. Zhan and Z. Huang, *Energy & Fuels*, 2020, **34**, 14757-14767.
36. T. V. Mai and L. K. Huynh, *Phys. Chem. Chem. Phys.*, 2019, **21**, 21162-21165.
37. T. V. T. Mai and L. K. Huynh, *New J. Chem.*, 2021, **(accepted)**.
38. T. V. T. Mai, H. T. Nguyen and L. K. Huynh, *Chemosphere*, 2020, **263**, 127850.
39. T. V. T. Mai and L. K. Huynh, *Phys. Chem. Chem. Phys.*, 2020, **22**, 25740-25746.
40. T. V.-T. Mai, T. T.-D. Nguyen, H. T. Nguyen, T. T. Nguyen and L. K. Huynh, *Environ. Sci. Technol.*, 2021, **55**, 7858-7868.
41. I. M. Alecu, J. Zheng, Y. Zhao and D. G. Truhlar, *J. Chem. Theory. Comput.*, 2010, **6**, 2872-2887.
42. C. Gonzalez and H. B. Schlegel, *J. Chem. Phys.*, 1989, **90**, 2154-2161.
43. C. Gonzalez and H. B. Schlegel, *J. Phys. Chem.*, 1990, **94**, 5523-5527.
44. M. v. Duong, H. T. Nguyen, N. Truong, T. N. M. Le and L. K. Huynh, *Int. J. Chem. Kinet.*, 2015, **47**, 564-575.
45. M. V. Duong, H. T. Nguyen, T. V. Mai and L. K. Huynh, *Phys. Chem. Chem. Phys.*, 2018, **20**, 1231-1239.
46. D. T. Gillespie, *J. Comput. Phys.*, 1976, **22**, 403-434.

47. D. T. Gillespie, A. Hellander and L. R. Petzold, *J. Chem. Phys.*, 2013, **138**, 170901-170914.
48. C. Eckart, *Phys. Rev.*, 1930, **35**, 1303-1309.
49. T. V. T. Mai, M. v. Duong, X. T. Le, L. K. Huynh and A. Ratkiewicz, *Struct. Chem.*, 2014, **25**, 1495-1503.
50. T. H. M. Le, S. T. Do and L. K. Huynh, *Comput. Theor. Chem.*, 2017, **1100**, 61-69.
51. T. H. M. Le, T. T. Tran and L. K. Huynh, *Chemom. Intell. Lab. Syst.*, 2018, **172**, 10-16.
52. T. Tan, X. Yang, Y. Ju and E. A. Carter, *J. Phys. Chem. B*, 2016, **120**, 1590-1600.
53. A. V. Joshi and H. Wang, *Int. J. Chem. Kinet.*, 2006, **38**, 57-73.
54. H. Hippler, *J. Chem. Phys.*, 1983, **78**, 6709.
55. Lawrence Livermore National Laboratory,
[https://combustion.llnl.gov/content/assets/docs/combustion/MCH tran dat.txt](https://combustion.llnl.gov/content/assets/docs/combustion/MCH_tran_dat.txt)).
56. T. Beyer and D. F. Swinehart, *Communications of the ACM*, 1973, **16**, 379.
57. J. W. Cooley and J. W. Tukey, *Math. Comput.*, 1965, **19**, 297-301.
58. S. H. Robertson, M. J. Pilling, D. L. Baulch and N. J. B. Green, *J. Phys. Chem.*, 1995, **99**, 13452-13460.
59. Y. Georgievskii and S. J. Klippenstein, *J. Chem. Phys.*, 2005, **122**, 194103-194117.
60. E. L. Daniel Grosjean, *Atmos. Environ.*, 1992, **26**, 1395-1405.
61. J. P. Senosiain, S. J. Klippenstein and J. A. Miller, *J. Phys. Chem. A*, 2006, **110**, 6960-6970.
62. J. Daranlot, A. Bergeat, F. Caralp, P. Caubet, M. Costes, W. Forst, J. C. Loison and K. M. Hickson, *Chem. Phys. Chem.*, 2010, **11**, 4002-4010.
63. R. Izsak, M. Szori, P. J. Knowles and B. Viskolcz, *J. Chem. Theory Comput.*, 2009, **5**, 2313-2321.
64. I. V. Tokmakov and M. C. Lin, *The journal of physical chemistry. A*, 2002, **106**, 11309-11326.
65. J.-C. Loison, M.-T. r. s. Rayez, J.-C. Rayez, A. Gratien, P. Morajkar, C. Fittschen and E. Villenave, *J. Phys. Chem. A*, 2012, **116**, 12189-12197.
66. M. Szori, T. Abou-Abdo, C. Fittschen, I. G. Csizmadia and B. Viskolcz, *Phys. Chem. Chem. Phys.*, 2007, **9**, 1931-1940.
67. J. Wu, H. Ning, L. Ma and W. Ren, *Phys. Chem. Chem. Phys.*, 2018, **20**, 26190-26199.
68. G. D. Purvis and R. J. Bartlett, *J. Chem. Phys.*, 1982, **76**, 1910-1918.
69. G. E. Scuseria, C. L. Janssen and H. F. Schaefer, *J. Chem. Phys.*, 1988, **89**, 7382-7387.
70. G. E. Scuseria and H. F. Schaefer, *J. Chem. Phys.*, 1989, **90**, 3700-3703.
71. A. Halkier, T. Helgaker, P. Jørgensen, W. Klopper, H. Koch, J. Olsen and A. K. Wilson, *Chem. Phys. Lett.*, 1998, **286**, 243-252.
72. E. E. Greenwald, S. W. North, Y. Georgievskii and S. J. Klippenstein, *J. Phys. Chem. A*, 2005, **109**, 6031-6044.
73. E. E. Greenwald, S. W. North, Y. Georgievskii and S. J. Klippenstein, *J. Phys. Chem. A*, 2007, **111**, 5582-5592.
74. Y. Georgievskii and S. J. Klippenstein, *J. Phys. Chem. A*, 2007, **111**, 3802-3811.
75. C. J. Nielsen, H. Herrmann and C. Weller, *Chem. Soc. Rev.*, 2012, **41**, 6684-6704.
76. B. D'Anna, V. Bakken, J. Are Beukes, C. J. Nielsen, K. Brudnik and J. T. Jodkowski, *Phys. Chem. Chem. Phys.*, 2003, **5**, 1790-1805.
77. J. Peeters, W. Boullart, V. Pultau, S. Vandenberg and L. Vereecken, *J. Phys. Chem. A*, 2007, **111**, 1618-1631.
78. D. Grosjean and E. L. Williams, *Atmos. Environ. Part A*, 1992, **26**, 1395-1405.